INTERNATIONAL JOURNAL OF INTEGRATED ENGINEERING
ISSN: 2229-838X e-ISSN: 2600-7916

IJIE

Vol. 16 No. 6 (2024) 206-215
https://publisher.uthm.edu.my/ojs/index.php/ijie

Mechanical Properties of Thulium-doped Bismuth Borotellurite Glass via Nanoindentation for Lead-Free Radiation Shielding Application

Nur Arina Mat Rusni[1,2], Azuraida Amat[2]*, Wan Yusmawati Wan Yusoff[2], Nor Azlian Abdul-Manaf[2], Nurazlin Ahmad[2]

[1] *Faculty of Defence Science and Technology,*
Universiti Pertahanan Nasional Malaysia, Kem Sungai Besi, 57000 Kuala Lumpur, MALAYSIA
[2] *Physics Department, Centre for Defence Foundation Studies,*
National Defense University of Malaysia, Kem Sungai Besi, 57000 Kuala Lumpur, MALAYSIA

*Corresponding Author: azuraida@upnm.edu.my
DOI: https://doi.org/10.30880/ijie.2024.16.06.020

Article Info

Received: 12 August 2024
Accepted: 9 October2024
Available online: 5 November 2024

Keywords

Thulium doped bismuth borotellurite glass; structural properties; mechanical properties; nanoindentation; Berkovich indenter

Abstract

Commercially, lead-based glasses are used in industry as transparent radiation shielding material due to their durability. However, lead toxicity could cause detrimental health issues to humans. Thus, in this study, a new composition of thulium-doped bismuth borotellurite glass was fabricated via melt-and-quench technique. The effect of bismuth oxide (Bi_2O_3) on the physical, structural, and mechanical properties of the glass was investigated. Glass with 0.25 mol% of Bi_2O_3 has the highest density. However, the oxygen packing density (OPD) of glass with 0.15 mol% of Bi_2O_3 is higher than 0.25 mol% of Bi_2O_3. This is due to a high number of non-bridging oxygen (NBOs) in 0.25 mol% of Bi2O3 glass structure. The bonds that are present in the glass structure were verified by Fourier Transform Infrared Spectroscopy (FTIR) analysis. Then, the mechanical properties were investigated by nanoindentation test with Berkovich indenter. Comparing the mechanical properties of indented glass samples, 0.15Bi glass projected the best mechanical durability since it provides the highest hardness and reduced elastic modulus value. Also, the low plastic work and optimal elastic work make 0.15Bi glass resilient to stress. Thus, the 0.15Bi glass is deemed as the best glass sample for high mechanical strength radiation shielding glass. This lead-free radiation shielding glass does not pose harmful effects to humans.

1. Introduction

Nowadays, lead-based glasses are abundantly used for photonic applications, especially in radiation shielding [1]. However, lead poses harmful effects to humans. Through ingestion of contaminated soil or dust, lead can be readily absorbed through the bloodstream and causes harmful effects on the central nervous system, cardiovascular system, kidneys, and immune system [2]. In China, specifically in Shaanxi and Hunan province, two lead poisoning cases involving 2000 children sparked riots due to a weak monitoring system of lead exposure levels in factories [3]. Nevertheless, lead-based glasses are still being chosen in medical and industrial application that requires transparent radiation shielding due to their high mechanical durability. The lead-based glasses have mechanical durability that is resistant to corrosion and does not degrade to other substances over time [4]. Although various research on radiation shielding properties has been done to replace high-density lead, there is still a lack of study on the durability of lead-free glass, especially on the mechanical properties. There is only one

piece of literature found on the investigation of radiation shielding glass by nanoindentation [5]. Consequently, it is hard to compare the mechanical durability of lead-free radiation shielding glass. Thus, to enable lead-free glass to be applied in industry, it is important to assess the mechanical strength of glass.

In this study, a new composition of lead-free glass was fabricated. The compound tellurium dioxide (TeO_2) was incorporated as the base-glass. Since TeO_2 is a conditional glass former, it is crucial to add dopants into the glass system. Incorporation of dopants results in stable tellurite-based glass formation with slow cooling rates [6]. However, the amorphous nature of TeO_2 glasses is still not fully understood unlike silicon dioxide (SiO_2). The coordination number of pure SiO_2 is 4 while recent nuclear magnetic resonance (NMR) spectroscopy showed the coordination number of TeO_2 is 3.9 [7]. This explains why it is difficult to produce a large quantity of tellurite-based glass. Thus, further experimental try-out of new composition needs to be done to produce structurally stable tellurite glass.

Boron oxide (B_2O_3) was also incorporated in the new glass composition. In lead-borate glass, it was found that the glass had high structural steadiness against up to 250 kGy of gamma radiation [8]. B_2O_3 compound also has the potential to be used on a large scale since it is low in cost and enables glass to be easily shaped [9]. Then, thulium (III) oxide (Tm_2O_3) was doped in the glass composition. Previous research found that thulium-doped glasses showed a significantly high linear attenuation coefficient compared to other rare-earth oxides such as erbium and holmium [10]. A high linear attenuation coefficient is desired in radiation shielding material since it indicates a high amount of incident photons attenuated per unit thickness of a material.

In this study, to investigate the effect of high-density bismuth oxide (Bi_2O_3), varying amounts of Bi_2O_3 was incorporated. In a study of bismuth lead borate glass, glass with the highest density resulted in good radiation shielding capability [11]. High-density materials are important for radiation shielding especially high penetration radiation such as gamma rays. This is because there will be a higher probability of atoms interaction with the gamma radiation. Thus, glass with the best radiation shielding capability would have the highest density.

Mainly, this study was conducted to investigate the mechanical properties of thulium-doped bismuth borotellurite glass by nanoindentation approach. This mechanical strength investigation would serve as a good reference for the application of lead-free radiation shielding glass on an industrial scale. To examine the effect of bismuth further, physical, and structural properties investigation also was conducted. The new composition of thulium-doped bismuth tellurite glass also does not pose harmful effects to humans.

2. Materials and Methods

2.1 Glass Samples Fabrication

Thulium-doped bismuth borotellurite glass was fabricated using the melt-and-quench technique method with the chemical composition of $[TeO_2)_{0.75}$ $(B_2O_3)_{0.25}]_{1-x}$ $(Bi_2O_3)_x$ $[Tm_2O_3]_{0.02}$ where x = 0.05, 0.15, 0.25 mol %. Table 1 shows the glass code and chemical composition of fabricated glass samples based on stoichiometric calculation. After the mass of each chemical compound was measured using PGW 214 analytical balance from AE Adam, the chemical compounds were mixed and grounded using mortar and pestle. Then, the grounded mixture was placed in an alumina crucible and underwent a pre-heat process at 400°C for an hour in an electrical furnace. Then, the pre-heated crucible was transferred to another furnace for a melting process for an hour at 900°C temperature. The molten sample was then poured onto a heated stainless-steel mould. Lastly, the poured sample underwent an annealing process at 400°C for an hour and was left to cool down at room temperature. Figure 1 shows the flowchart of the fabrication methodology and Figure 2 represents the fabricated glass samples.

Table 1 *Glass code and chemical composition of prepared glass samples*

Glass Code	Chemical Composition				
	TeO_2	B_2O_3	Bi_2O_3	Tm_2O_3	TeO_2
0.05Bi	0.702	0.102	0.147	0.049	0.702
0.15Bi	0.519	0.075	0.365	0.040	0.519
0.25Bi	0.390	0.057	0.519	0.034	0.390

2.2 Physical Properties

A density meter was used to investigate the density of the prepared glasses. By implementing Archimedes's Principle, the density of glass (ρ_{glass}) was calculated using equation (1).

$$\rho_{glass} = \left(\frac{w_{air}}{w_{air} - w_{water}}\right)(\rho_{water}) \quad (1)$$

Int. Journal of Integrated Engineering Vol. 16 No. 6 (2024) 206-215

The symbols ρ_{water}, w_{air} and w_{water} represent the density of distilled water, the weight of the glass sample in air, and the weight of the glass sample in distilled water, respectively. Using the ρ_{glass} value, the molar volume (V_m) of the glass was calculated using equation (2).

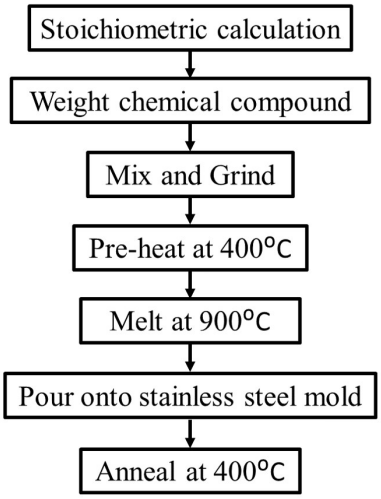

Fig. 1 *Flow chat fabrication of thulium doped bismuth borotellurite glass*

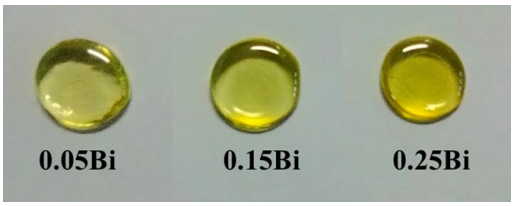

Fig. 2 *Fabricated glass samples*

$$V_m = \left(\frac{M_m}{\rho_{glass}}\right) \tag{2}$$

The symbol M_m represents the relative molar mass of glass samples. Then, oxygen bonds in the prepared glasses were evaluated by the calculation of oxygen packing density (OPD) with the equation as follows.

$$OPD = 1000 \times O \times \left(\frac{1}{V_m}\right) \tag{3}$$

Where O is the number of oxygens in the glass composition.

2.3 Structural Properties

Fourier Transform Infrared Spectroscopy (FTIR) analysis was conducted using Perkin Elmer Spectrum 100 FT-IR Spectrometer to investigate the structural properties of prepared glasses. The solid glass samples were analyzed in a range between 600cm^{-1} to 1500 cm^{-1}. The transmission spectrum of FTIR was studied to verify the chemical bonds that are present in the glass composition.

2.4 Nanoindentation Procedure

Thulium-doped bismuth tellurite glass samples were polished using 600, 2000, and 5000 grid sandpaper to obtain a flat and smooth surface before the nanoindentation procedure was done. All glass samples were polished to a thickness of about 4 mm. Then, the glass samples were cleaned using distilled water and acetone. The nanoindentation test was conducted using the Nano Test Vantage (Micro Materials Ltd) machine. Diamond Berkovich indenter was used, and the load-controlled mode was applied. The maximum load applied was 500 mN with 5 second dwell time at the maximum load. The loading and unloading rates were 50 mN/s. The frame compliance was 0.402 nm/Mn. Five indentations were done on each sample.

2.5 Mechanical Properties Calculation

Based on the nanoindentation results, load-displacement curves were plotted, and mechanical properties were investigated based on the curves. Then, mechanical properties such as maximum depth, hardness, reduced elastic modulus, elastic work, and plastic work were obtained from the nanoindentation instrument directly. Other mechanical properties such as contact stiffness (S), contact depth (h_c), and projected contact area (A_p), were calculated manually. S was determined based on the maximum penetration depth (h_{max}) and the unloading slope $\left(\frac{dF}{dh}\right)$ of the load-displacement curve from the nanoindentation tests as shown in Figure 3 S was determined based on the penetration depth displacement (Δh) and load difference (ΔF) of the unloading slope for the nanoindentation load-displacement [12,13].

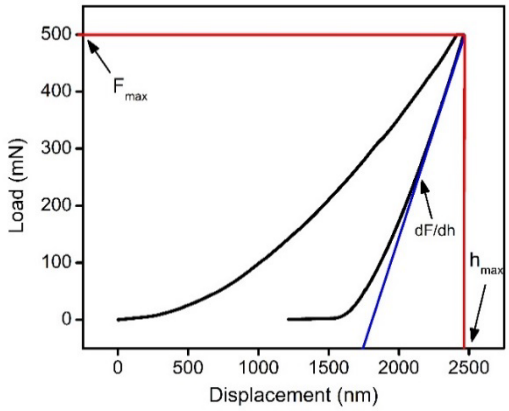

Fig. 3 *Loading and unloading slope of load-displacement curves*

$$S = \frac{\Delta F}{\Delta h} = \frac{dF}{dh} \tag{4}$$

The h_c is the value that shows the depth of the indenter tip that came into contact with the surface of the sample. Using the Oliver-Pharr equation, h_c was evaluated as follows [14,15].

$$h_c = h_{max} - \varepsilon \frac{F_{max}}{S} \tag{5}$$

Where h_{max}, ε, and F_{max} is the maximum penetration depth, indenter-constant, and maximum force, respectively. Indenter-constant (ε) for Berkovich indenter is 0.72 [14]. Then, using the value of h_c, the A_p was calculated using Equation (3) as follows [16].

$$A_p = 24.5\ {h_c}^2 \tag{6}$$

3. Results and Discussions

3.1 Physical Properties

Table 2 shows the density and molar volume of investigated glass samples. Based on the density results, as the amount of Bi_2O_3 increases, the density of the glass also increases. The addition of heavier Bi_2O_3 compounds replaced the lighter compounds in the glass system making the overall density of the glass increase. In radiation shielding application, the material with the highest density, which in this case is 0.25Bi glass would provide the best radiation shielding capability. This is because high-density materials would provide a high probability of atom interactions [17]. The rise in density also can be attributed to the rearrangement of the glass structure. Theoretically, the relationship between density and molar volume should be inversely proportional as shown in equation (2). However, the investigated glass samples showed contradictory behaviour where the molar volume increases with density as shown in Table 2. The contradicting behaviour is due to an increment in interatomic spacing atoms. The ionic radii of modifier Bi^{3+} ions (140pm) are bigger than the Te^{2+} (74pm), and B^{3+} (85pm) ions in the glass composition. Hence, this resulted in the creation of free excess volume in the glass network when a higher number of Bi^{3+} ions was incorporated into the glass structure [18]. The 0.15Bi glass resulted in the highest oxygen packing density (OPD). This is due to optimum Bi_2O_3 incorporated in the glass composition that acts as a network former. Excessive addition of Bi_2O_3 caused the number of non-bridging oxygen (NBO) to increase [19]. This causes the glass to be less compact as depicted in OPD of 0.25Bi glass.

Int. Journal of Integrated Engineering Vol. 16 No. 6 (2024) 206-215

Table 2 *Glass code, density, molar volume, and oxygen packing density of thulium doped bismuth borotellurite glass*

Glass Code	Density (g/cm^3)	Molar Volume (cm^3/mol)	Oxygen Packing Density (g/cm^3)
0.05Bi	4.811	32.950	69.742
0.15Bi	5.676	33.722	73.483
0.25Bi	6.200	36.176	72.147

3.2 Structural Properties

FTIR analysis was conducted to evaluate the chemical bonds that are present in the glass system. Figure 4 presents the FTIR spectra of fabricated thulium-doped bismuth tellurite glass. A transmittance peak was observed at 619 cm^{-1}, 622 cm^{-1}, and 624 cm^{-1} indicating the vibrations of Bi–O–Bi and Bi–O bonds for BiO_6 octahedral units in 0.05Bi, 0.15Bi, and 0.25Bi glass, respectively [20]. Then, a respective peak at 648 cm^{-1}, 664 cm^{-1}, and 689 cm^{-1} in 0.05Bi, 0.15Bi, and 0.25Bi glass represents the stretching vibration of Te-O in TeO_3 units [21]. Comparing the Te-O and Bi-O peaks in the FTIR transmittance spectra, it is observed that the peaks appear more prominent and broader in 0.15Bi glass than in 0.05Bi and 0.25Bi glass. This could be due to a high number of bridging oxygen (BO) 0.15Bi glass which resulted in a high number of Te-O and Bi-O bonds. The results of *OPD* verify this claim. As mentioned earlier, the 0.15Bi glass resulted in a higher *OPD* than 0.05Bi and 0.25Bi glass due to a high number of BO that makes the glass structure more dense than other fabricated glass samples. Furthermore, a small peak was observed at wavenumber 901 cm^{-1} which represents the stretching vibration of BO_4 tetrahedra units [21–23]. Sharper peaks at 1215 cm^{-1}, 1368 cm^{-1}, and 1440 cm^{-1} were due to stretching vibrations of trigonal BO_3 units [24,25]. This indicates that most B_2O_3 retain their trigonal BO_3 trigonal structural units rather than forming extra BO to form BO_4 tetrahedra units [26].

3.3 Mechanical Properties

The representative load-displacement curves for thulium-doped bismuth tellurite glass using the Berkovich indenter are displayed in Figure 5. The indentation was performed at five different indentation sites. The loading and unloading curves for each glass sample agree well with each other. This indicates the homogenous nature of glass samples. Based on the loading curves, no noticeable pop-ins observed. The absence and presence of pop-ins were due to shear bands on the surface of deformation zones. According to the results obtained with Pd-Si glass, a primary shear band (PSB) caused the pop-ins in the load-displacement curves [27]. Meanwhile, a secondary shear band (SSB) cannot be observed from the curves due to indentation machine limitation.

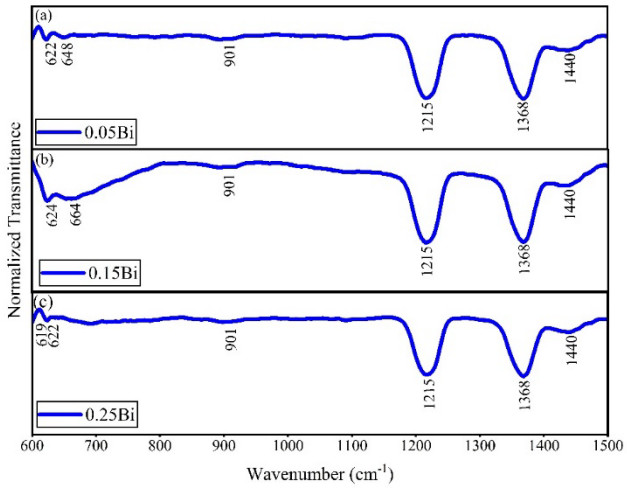

Fig. 4 *FTIR spectra (a) 0.05Bi; (b) 0.15Bi; and 0.25Bi glass at wavenumber 600 cm^{-1} to 1500 cm^{-1}*

Figure 6(a) portrays the plot of load versus average displacement curve of thulium-doped bismuth borotellurite glasses at Bi_2O_3 concentration. When comparing the displacement curves of 0.05Bi, 0.15Bi, and 0.25Bi glass samples, a shift in load-displacement curves was observed. When the amount of Bi_2O_3 incorporation increases from 0.05 mol% to 0.15 mol %, the graph shifts to the left due to lower penetration depth in 0.15Bi glass than 0.05Bi. Then, the load-displacement curve shifted to the right when 0.25 mol % of Bi_2O_3 was incorporated due to high penetration depth. This shift in load-displacement curves also was observed in Al_3Zr crystal embedded in aluminium, polycrystalline, and cement matrix [28]. Al_3Zr crystal embedded in cement matrix has the highest penetration depth when compared to Al_3Zr crystal embedded in aluminium, and polycrystalline. Hence, the Al_3Zr

crystal embedded in the cement matrix was located at the rightest part of the load-displacement curve. Figure 6(b) shows the zoomed-in view of the unloading curves. Pop-outs can be observed at load 50 mN for every indented glass sample as depicted in Figure 6(b) by arrows. Similar pop-outs also were observed in single-crystal Si where pop-outs occur at load 30mN [12]. In single-crystal silicon (Si), the pop-outs occur due to a phase transformation of crystal to amorphous Si [29,30]. When observed under transmission electron microscopy (TEM), and selected area diffraction (SAD), a mixture of amorphous Si and crystalline Si were observed [12]. Thus, it can be inferred that the presence of pop-outs in the fabricated glasses was due to the presence of amorphous and crystalline phases in the glass structure.

Table 3 *Summary of FTIR spectra bands position and assignments for thulium doped bismuth tellurite glass*

Wavenumber (cm^{-1})	Assignments
622 (a) 624 (b) 619 (c)	Bi–O–Bi and Bi–O in BiO_6 octahedral [20]
648 (a) 664 (b) 622 (c)	TeO_3 stretching vibration [21]
901	Stretching vibration BO_4 tetrahedra units [21–23]
1215 1368 1440	Stretching vibration of trigonal BO_3 units [24,25]

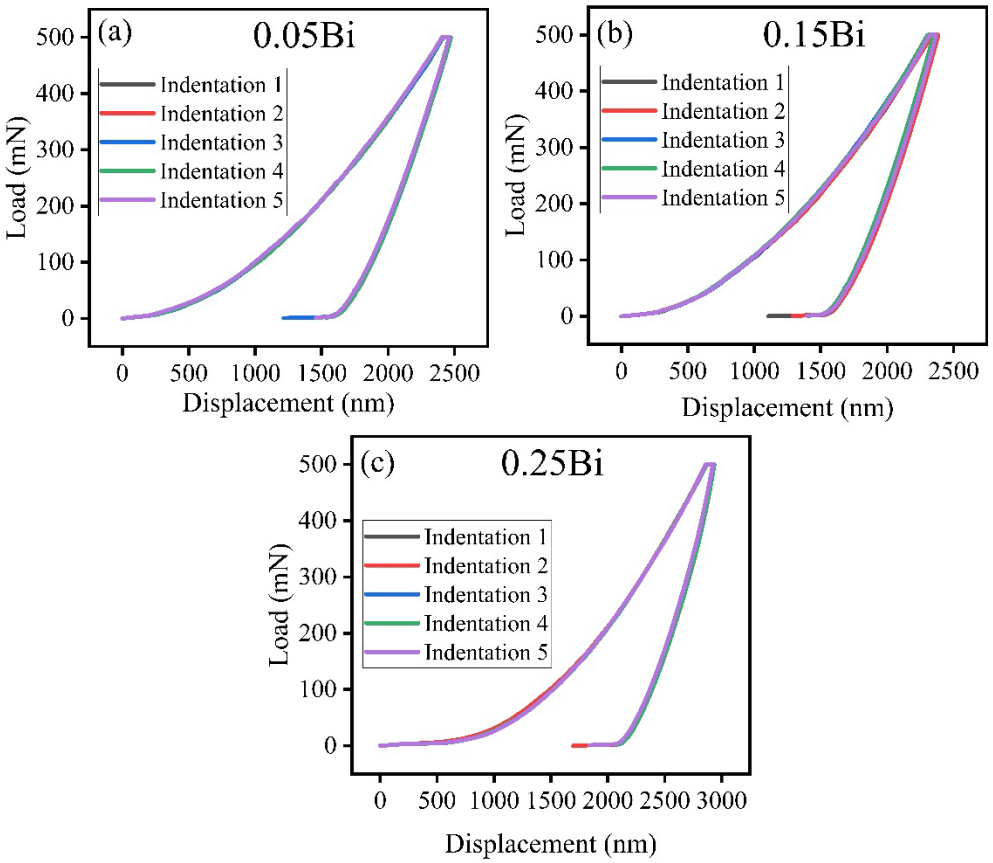

Fig. 5 *Load-displacement curves of thulium doped bismuth borotellurite glasses at five different indentation sites*

The hardness and reduced elastic modulus of fabricated glass samples are shown in Figure 7. Hardness can be described as the resistance toward local deformation [31]. In the case of this study, the hardness of a material is the average stress on the surface of indented glass. As for reduced modulus, it is a combination of the sample material and indenter elastic deformations [32]. Based on the results, the 0.15Bi glass sample shows the highest value of hardness compared to 0.05Bi and 0.25Bi glasses. The high value of hardness is because the 0.15Bi glass sample has the highest number of network connectivity. Since the hardness of a glass is dependent on network connectivity, the presence of a high number of NBOs reduces the hardness of the glass [33]. The 0.25Bi glass has a high number of NBOs based on the result of *OPD* tabulated in Table 2. Then, the reduced elastic modulus of

Int. Journal of Integrated Engineering Vol. 16 No. 6 (2024) 206-215

fabricated glass samples was compared. The 0.15Bi glass shows a significantly high value of reduced elastic modulus. The high reduced elastic modulus is due to the strong interatomic force and *OPD* in the glass structure [34]. Since the 0.15Bi glass has a lower number of NBOs than other prepared glass samples, it showed that the 0.15Bi glass is tightly packed thus resulting in a high *OPD*. Meanwhile, low reduced elastic modulus occurred due to the high number of broken bonds in the glass structure [35]. In the case of 0.25Bi glass, the broken bonds of NBOs caused its low reduced elastic modulus. Generally, 0.15Bi glass is the best glass sample in terms of hardness and reduced elastic modulus. It was clear that the incorporation of Bi_2O_3 would enhance the hardness and the reduced elastic modulus of the glass system. However, Bi_2O_3 should not be added excessively since it would increase the NBOs which results in decreasing hardness and reduced elastic modulus of the glass system.

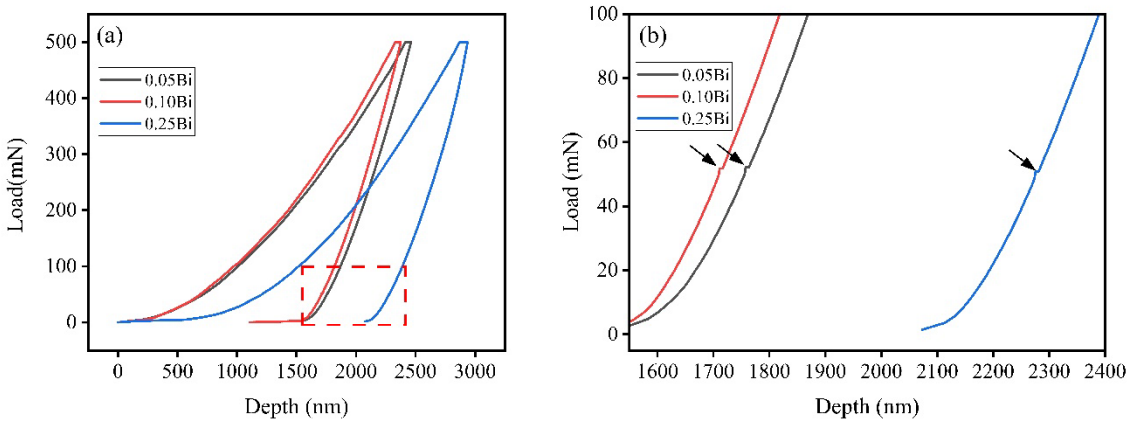

Fig. 6 *(a) Load-displacement curves; and (b) zoom-in view of pop-outs of unloading curves of thulium doped bismuth tellurite glass with varying Bi_2O_3 concentration*

The term "stiffness" refers to the amount of force required to cause a specific deformation in a structure [36]. Based on the results in Table 3, 0.05Bi glass results in the lowest stiffness value compared to 0.15Bi and 0.25Bi glass. The trend stiffness does not correlate with hardness as shown in the previous study where the concept of low stiffness would result in high hardness [37]. However, the calculated contact depth and projected area using the value of stiffness showed a direct relationship with hardness where low indentation contact depth was due to high hardness. As shown in Table 3, 0.15Bi which poses the highest hardness resulted in the lowest contact depth.

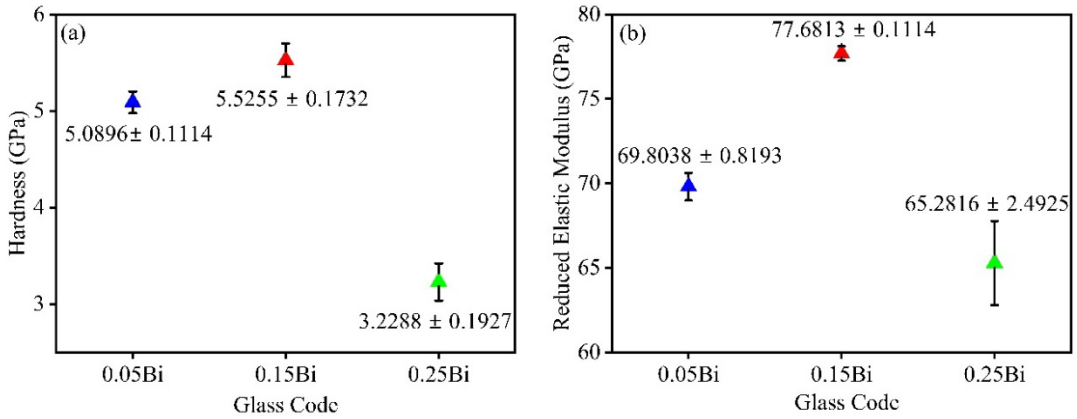

Fig. 7 *(a) Hardness; and (b) reduced elastic modulus with error bars of thulium doped bismuth borotellurite glasses*

Table 3 *Stiffness, contact depth and projected area of thulium doped bismuth borotellurite glass*

Glass Code	Hardness (GPa)	Reduced Modulus (GPa)	Stiffness (mN/nm)	Contact Depth (nm)	Projected Area (nm^2) ($\times 10^7$)
0.05Bi	5.0896	69.8083	0.7821	2007.00	9.8687
0.15Bi	5.5255	77.6813	0.8511	1934.32	9.1669
0.25Bi	3.2288	65.2816	0.9271	2524.07	15.6088

Figure 8 shows the graph of elastic and plastic work of thulium-doped bismuth borotellurite glass. It is worth noting that the value of hardness correlates well with the value of plastic work [38]. When the hardness of a material increased, the plastic work decreased as projected in Figure 8(a). It is also found that the 0.15Bi glass sample has the lowest plastic work compared to other investigated glass samples. This means that 0.15Bi glass is the least likely to undergo permanent deformation. As for elastic work, a good correlation between elastic work and stiffness was observed. The decreasing stiffness of a material indicates that the elastic work increases. Based on the result in Figure 8(b), 0.05Bi glass has the highest elastic work compared to other glass samples. Thus, it shows that 0.05Bi glass is resilient and able to withstand the highest amount of stress before permanent deformation occurs. Comparing the elastic-plastic behaviour of prepared glasses, 0.15Bi glass is the best glass sample in terms of mechanical durability since the indentation resulted in the lowest plastic work and optimal elastic work.

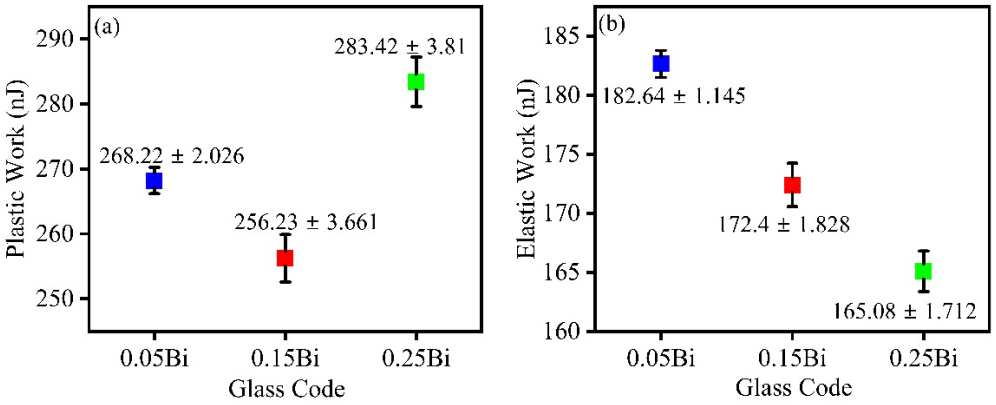

Fig. 8 *(a) Plastic work; and (b) Elastic work with error bars of thulium doped bismuth borotellurite glasses*

4. Conclusion

In this study, the mechanical properties of thulium-doped bismuth borotellurite radiation shielding glass were investigated using a nanoindentation test with Berkovich indenter. The load-displacement curve of the nanoindentation at five different indentation sites agrees well with each other indicating that the prepared glass is homogenous. Pop-outs were observed on the unloading curves of all glass samples due to a phase transformation of crystals to amorphous. Comparing the mechanical properties of indented glass samples, 0.15Bi glass projected the best mechanical durability since it provides the highest hardness and reduced elastic modulus value. Material with high hardness resulted in low contact depth and low projected area value as depicted by 0.15Bi glass. Also, the low plastic work and optimal elastic work make 0.15Bi glass resilient to stress before permanent deformation occurs. Thus, the 0.15Bi glass is deemed to be the best glass sample in terms of mechanical strength. This lead-free glass is eco-friendly and has the potential to replace lead glass in radiation shielding applications.

Acknowledgement

This study had been supported by Malaysian Ministry of Higher Education (MoHE) Malaysia under the scholarship of MyBrainSc and National Defense University of Malaysia (NDUM) with GPJP grant (UPNM/2022/GPJP/SG/3). Authors are incredibly grateful for all the support that has been given.

Conflict of Interest

Authors declare that there is no conflict of interests regarding the publication of the paper.

Author Contribution

This journal requires that all authors take public responsibility for the content of the work submitted for review. The contributions of all authors must be described in the following manner: *The authors confirm contribution to the paper as follows:* ***study conception and design:*** *Nur Arina Mat Rusni, Azuraida Amat, Wan Yusmawati Wan Yusoff;* ***data collection:*** *Nur Arina Mat Rusni;* ***analysis and interpretation of results:*** *Nur Arina Mat Rusni;* ***draft manuscript preparation:*** *Nur Arina Mat Rusni, Azuraida Amat, Wan Yusmawati Wan Yusoff, Nor Azlian Abdul-Manaf, Nurazlin Ahmad. All authors reviewed the results and approved the final version of the manuscript.*

References

[1] Mohammed, R. Y., Ahmed, F. K., Abdulrahman, A. F., Hamad, S. M., Ahmed, S. M., Barzinjy, A. A., & Almessiere, M. A. (2023). Impact of growth temperature of lead-oxide nanostructures on the attenuation of gamma radiation. *ACS omega*, *8*(24), 22230-22237. https://doi.org/10.1021/acsomega.3c02910 .

[2] Ara, A., & Usmani, J. A. (2015). Lead toxicity: a review. *Interdisciplinary toxicology*, *8*(2), 55-64. https://doi.org/10.1515/intox-2015-0009.

[3] Watts, J. (2009). Lead poisoning cases spark riots in China. *The Lancet*, *374*(9693), 868. https://doi.org/10.1016/S0140-6736(09)61612-3.

[4] Naranjo, V. I., Hendricks, M., & Jones, K. S. (2020). Lead toxicity in children: an unremitting public health problem. *Pediatric Neurology*, *113*, 51-55. https://doi.org/10.1016/j.pediatrneurol.2020.08.005.

[5] Wakui, T., Yamasaki, K., & Futakawa, M. (2022). Material properties evaluation on radiation shielding lead glasses irradiated by pulsed laser. *Advanced Experimental Mechanics*, *7*, 103-109. https://doi.org/10.11395/aem.7.0_103

[6] Jha, A., Richards, B. D. O., Jose, G., Toney Fernandez, T., Hill, C. J., Lousteau, J., & Joshi, P. (2012). Review on structural, thermal, optical and spectroscopic properties of tellurium oxide based glasses for fibre optic and waveguide applications. *International Materials Reviews*, *57*(6), 357-382. https://doi.org/10.1179/1743280412Y.0000000005.

[7] Hauke, B., Barney, E.R., Pakhomenko, E., Jesuit, M., Packard, M., Crego, A., Tarantino, G., Affatigato, M. and Feller, S., (2020). Structure and glass transition temperatures of tellurite glasses. *Physics and Chemistry of Glasses-European Journal of Glass Science and Technology Part B*, *61*(1), 21-26. https://doi.org/10.13036/17533562.61.1.11.

[8] Abou Hussein, E. M., & Madbouly, A. M. (2024). Fabrication and characterization of different PbO borate glass systems as radiation-shielding containers. *Scientific Reports*, *14*(1), 2638. https://doi.org/10.1038/s41598-024-52071-x.

[9] Abouhaswa, A. S., Rammah, Y. S., Ibrahim, S. E., & El-Mallawany, R. (2019). Optical and electrical properties of lead borate glasses. *Journal of Electronic Materials*, *48*, 5624-5631. https://doi.org/10.1007/s11664-019-07391-4.

[10] Vani, P., Vinitha, G., Sayyed, M. I., AlShammari, M. M., & Manikandan, N. (2021). Effect of rare earth dopants on the radiation shielding properties of barium tellurite glasses. *Nuclear Engineering and Technology*, *53*(12), 4106-4113. https://doi.org/10.1016/j.net.2021.06.009.

[11] Saleh, E. E., Algradee, M. A., El-Fiki, S. A., & Youssef, G. M. (2022). Fabrication of novel lithium lead bismuth borate glasses for nuclear radiation shielding. *Radiation Physics and Chemistry*, *193*, 109939. https://doi.org/10.1016/j.radphyschem.2021.109939.

[12] Olasz, D., Lendvai, J., Szállás, A., Gulyás, G., & Chinh, N. Q. (2020). Extended applications of the depth-sensing indentation method. *Micromachines*, *11*(11), 1023. https://doi.org/10.3390/mi11111023.

[13] Loubet, J. L. (1995). Some measurements of viscoelastic properties with the help of nanoindentation. In *Extended Abstracts, Proc. Workshop on Indentation Techniques, ICMCTF-95, San Diego, CA*. https://doi.org/10.6028/jres.101.010.

[14] Oliver, W. C., & Pharr, G. M. (1992). An improved technique for determining hardness and elastic modulus using load and displacement sensing indentation experiments. *Journal of materials research*, *7*(6), 1564-1583. http://www.journals.cambridge.org/abstract%7B_%7DS0884291400017039.

[15] Chen, D. Q., Zhou, G. Y., Liu, Z. P., & Tu, S. T. (2015). Nanoindentation experimental study on mechanical properties of as-cast BNi-2 solder alloy. *Procedia Engineering*, *130*, 652-661. https://doi.org/10.1016/j.proeng.2015.12.289.

[16] Gong, J., Miao, H., & Peng, Z. (2004). On the contact area for nanoindentation tests with Berkovich indenter: case study on soda-lime glass. *Materials letters*, *58*(7-8), 1349-1353. https://doi.org/10.1016/j.matlet.2003.09.026.

[17] Akyildirim, H., Kavaz, E., El-Agawany, F. I., Yousef, E., & Rammah, Y. S. (2020). Radiation shielding features of zirconolite silicate glasses using XCOM and FLUKA simulation code. *Journal of Non-Crystalline Solids*, *545*, 120245. https://doi.org/10.1016/j.jnoncrysol.2020.120245.

[18] Effendy, N., Ab Aziz, S. H., Kamari, H. M., Zaid, M. H. M., Budak, C. E. A., Shabdin, M. K., ... & Wahab, S. A. A. (2020). Artificial neural network prediction on ultrasonic performance of bismuth-tellurite glass compositions. *Journal of Materials Research and Technology*, *9*(6), 14082-14092. https://doi.org/10.1016/j.jmrt.2020.09.107.

[19] Alshamari, A., Mhareb, M.H.A., Alonizan, N., Sayyed, M.I., Dwaikat, N., Alrammah, I., Hamad, M.K. and Drmosh, Q.A., (2023). Gamma-ray-induced changes in the radiation shielding, structural, mechanical, and optical properties of borate, tellurite, and borotellurite glass systems modified with barium and bismuth oxide. *Optik*, *281*, 170829. https://doi.org/10.1016/j.ijleo.2023.170829.

[20] Oo, H. M., Mohamed-Kamari, H., & Wan-Yusoff, W. M. D. (2012). Optical properties of bismuth tellurite based glass. *International journal of molecular sciences*, *13*(4), 4623-4631. https://doi.org/10.3390/ijms13044623.
[21] Halimah, M. K., Hasnimulyati, L., Zakaria, A., Halim, S. A., Ishak, M., Azuraida, A., & Al-Hada, N. M. (2017). Influence of gamma radiation on the structural and optical properties of thulium-doped glass. *Materials Science and Engineering: B*, *226*, 158-163. https://doi.org/10.1016/j.mseb.2017.09.010.
[22] Stoch, L., & Środa, M. (1999). Infrared spectroscopy in the investigation of oxide glasses structure. *Journal of molecular structure*, *511*, 77-84. https://doi.org/10.1016/S0022-2860(99)00146-5.
[23] Kaur, N., & Khanna, A. (2014). Structural characterization of borotellurite and alumino-borotellurite glasses. *Journal of non-crystalline solids*, *404*, 116-123. https://doi.org/10.1016/j.jnoncrysol.2014.08.002.
[24] Chowdari, B. V. R., & Rong, Z. (1996). The role of Bi_2O_3 as a network modifier and a network former in xBi2O3·(1− x) LiBO2 glass system. *Solid State Ionics*, *90*(1-4), 151-160. https://doi.org/10.1016/s0167-2738(96)00411-0.
[25] Kaur, A., Khanna, A., Bhatt, H., Gónzález-Barriuso, M., González, F., Chen, B., & Deo, M. N. (2017). BO and TeO speciation in bismuth tellurite and bismuth borotellurite glasses by FTIR, 11B MAS-NMR and Raman spectroscopy. *Journal of Non-Crystalline Solids*, *470*, 19-26. https://doi.org/10.1016/j.jnoncrysol.2017.04.028.
[26] Matsuda, Y., Fukawa, Y., Kawashima, M., Mamiya, S., & Kojima, S. (2008). Dynamic glass transition and fragility of lithium borate binary glass. *Solid State Ionics*, *179*(40), 2424-2427. https://doi.org/10.1016/j.ssi.2008.09.011.
[27] Sharma, A., Tripathi, A., Nandam, S. H., Hahn, H., & Prasad, K. E. (2023). Role of indenter geometry on the deformation behavior in a Pd-Si based metallic and nanoglass. *Journal of Alloys and Compounds*, *933*, 167693. https://doi.org/10.1016/j.jallcom.2022.167693.
[28] Priyadarshi, A., Subroto, T., Nohava, J., Pavel, S., Conte, M., Pericleous, K., Eskin, D., & Tzanakis, I. (2023). Investigation of mechanical properties of Al_3Zr intermetallics at room and elevated temperatures using nanoindentation. *Intermetallics*, *154*, 107825. https://doi.org/10.1016/j.intermet.2023.107825.
[29] Jiapeng, S., Cheng, L., Han, J., Ma, A., & Fang, L. (2017). Nanoindentation induced deformation and pop-in events in a silicon crystal: molecular dynamics simulation and experiment. *Scientific reports*, *7*(1), 10282. https://doi.org/10.1038/s41598-017-11130-2.
[30] Wang, S., Liu, H., Xu, L., Du, X., Zhao, D., Zhu, B., Yu, M. and Zhao, H., (2017). Investigations of phase transformation in monocrystalline silicon at low temperatures via nanoindentation. *Scientific Reports*, *7*(1), 8682. https://doi.org/10.1038/s41598-017-09411-x.
[31] Fan, J., Jiang, D., Zhang, H., Hu, D., Liu, X., Fan, X., & Zhang, G. (2022). High-temperature nanoindentation characterization of sintered nano-copper particles used in high power electronics packaging. *Results in Physics*, *33*, 105168. https://doi.org/10.1016/j.rinp.2021.105168.
[32] Shuman, D. J., Costa, A. L., & Andrade, M. S. (2007). Calculating the elastic modulus from nanoindentation and microindentation reload curves. *Materials characterization*, *58*(4), 380-389. https://doi.org/10.1016/j.matchar.2006.06.005.
[33] Yaacob, S. S., Mohd-Noor, F., Mawlud, S. Q., Aziz, S. M., Yusoff, N. M., Yusof, N. N., & Safaai, S. S. (2023). Correlation between structural and mechano-optical response of modified europium in magnesium borotellurite glass. *Journal of Non-Crystalline Solids*, *600*, 122010. https://doi.org/10.1016/j.jnoncrysol.2022.122010.
[34] Chen, M., Liu, J., & Wu, Z. (2022). Effect of Fe_2O_3 concentration on the properties of basalt glasses. *Journal of Natural Fibers*, *19*(2), 575-585. https://doi.org/10.1080/15440478.2020.1758277.
[35] Lee, C. S., Amin Matori, K., Ab Aziz, S. H., Kamari, H. M., Ismail, I., & Mohd Zaid, M. H. (2017). Comprehensive study on elastic moduli prediction and correlation of glass and glass ceramic derived from waste rice husk. *Advances in Materials Science and Engineering*, *2017*(1), 8962986. https://doi.org/10.1155/2017/8962986.
[36] Baumgart, E. (2000). Stiffness—an unknown world of mechanical science. *Injury*, *31*(Suppl 2), B14-23. https://doi.org/10.1016/S0020-1383(01)00057-2.
[37] Christensen, J. F., Krishnan, N. A., Bauchy, M., & Smedskjaer, M. M. (2023). Indenting glasses with indenters of varying stiffness and sharpness. *Journal of Non-Crystalline Solids*, *603*, 122111. https://doi.org/10.1016/j.jnoncrysol.2022.122111.
[38] Jha, K. K., Suksawang, N., & Agarwal, A. (2014). A new insight into the work-of-indentation approach used in the evaluation of material's hardness from nanoindentation measurement with Berkovich indenter. *Computational materials science*, *85*, 32-37. https://doi.org/10.1016/j.commatsci.2013.12.005.